Supplemental Information

Inventory of Supplemental Information

The following supplemental figures, tables, methods and references provide additional information supporting the characterization of the effects of resveratrol on cardiovascular function in high-fat, high-sucrose diet-fed rhesus monkeys.

Supplemental Methods

Supplemental data. *Tables S3A, S3B and S3C can be found as excel files.

Figure S1, related to Figure 3C- Change in expression of select genes between HFS vs. SD and HFS+R vs. HFS is depicted as Z-ratios.

Figure S2, related to Figure 4C- SILAC-based identification and quantitation of relative differential changes in protein expression from a primary culture of rhesus monkey vascular smooth muscle cells.

Figure S3, related to Figure 4D- Tissue transglutaminase activity in primary culture of rhesus monkey vascular smooth muscle cells.

Table S1, related to Figure 1 - Baseline characteristics of rhesus monkeys.

Table S2, Related to Figure 2 - Weight and dimensions of the heart, aortic remodeling, and semi-quantification scoring for fat deposition and calcification of the thoracic aorta following 2 years on study.

*Table S3A, related to Figure 3B - List of shared GO terms that were significantly affected both by HFS vs. SD and resveratrol in HFS+R vs. HF.

*Table S3B, related to Figure 3C- List of genes whose expression in HFS diet was reversed upon resveratrol supplementation.

*Table S3C, related to Figure 4A - SILAC-based identification and quantitation of relative differential changes in protein expression from a primary culture of rhesus monkey vascular smooth muscle cells.

Table S4, related to Figure 4A - Enrichment analysis of proteins that are significantly regulated by HFS/HFS+R within GO term-Biological Process, KEGG signaling pathways, WikiPathways, and PathwayCommons.

Supplemental Experimental Procedures

Table S5, related to Figure 3D – List of monkey primer sets for real-time PCR

Supplemental References

Supplemental Methods:

Animals

Twenty-four adult (7-13 years old) male rhesus monkeys (*Macaca mulatta*) were housed continuously at the NIH Animal Center, Poolesville, MD. All animals were considered healthy with no cardiovascular abnormalities. The animal center is fully accredited by the American Association for Accreditation of Laboratory Animal Care. All procedures were approved by the Animal Care and Use Committee of the NIA Intramural Program.

Housing

Monkeys were housed individually in standard nonhuman primate caging on a 12h light/12h dark cycle, room temperature (78±2 ^{o}F), and humidity at 60±20%. One pairing was maintained throughout the study; all other monkeys had extensive visual, auditory, and olfactory but limited tactile contact with monkeys housed in the same room. Monkeys received 2 meals per day at estimated *ad libitum* levels throughout the study. Water was always available *ad libitum*. Monkeys were monitored minimally 3 times daily by trained animal care staff.

Diet and Experimental Groups

During baseline assessments, all monkeys were maintained on a commercially available closed formula monkey chow (TestDiet®#5038 Purina Mills, Richmond, IN). After baseline assessment, the twenty four male rhesus monkeys were quasi- randomized into one of three groups: a high fat/high sucrose (HFS) diet (n=10); a HFS diet supplemented with resveratrol (HFS+R) (n=10); or, remaining on the healthy standard diet (SD) (n=4). The standard diet was a commercially available closed formula monkey chow (TestDiet #5038; Purina Mills), with 13% of kcal in fat and 2.24% sucrose by weight. The main sources of macronutrients in the SD were as follows: protein (soy meal, corn); fat (porcine fat, corn); carbohydrate (corn, wheat middlings). The HFS diet was a specially formulated, purified -ingredient diet with 42% kcal in fat and approximately 27% sucrose by weight (Custom formula #07802; Harlan, Teklad, Madison, WI). The main sources of macronutrients in the HFS diet were as follows: protein (casein, lactalbumin); fat (milk fat, soybean oil); carbohydrate (sucrose, maltodextrin). Macronutrient compositions in both diets as a percentage of kcals were as follows: (1) SD diet: 18.2% protein, 13.1% fat, 68.7% carbohydrate; (2) HFS diet: 15.8% protein, 42.3% fat, 41.9% carbohydrate. The monkeys were gradually switched to the HFS diet over a 3-week period. All groups received 2 meals per day of the specified diet in allotments that represent *ad libitum* feeding. Documentation of food consumption by individual animals throughout the study indicated that there was no difference in average consumption between groups on a per kg body

weight basis.

Resveratrol and Dose Determination

Resveratrol was supplied by DSM Nutritional Products (Parsippany, NJ). The dosing for monkeys was derived from the protective dose reported in mice (22 mg/kg) (Baur et al., 2006) and adjusted by allometric scaling to an average monkey body weight of 12.1 kg. The monkey equivalent dose was determined to be 40.7 mg. To confirm the allometric calculation, high performance liquid chromatography (HPLC) was applied on serum samples from resveratrol-fed mice; unmodified resveratrol was not detected but the metabolite, 3-*O*-glucuronide, was consistently identified. Next, a range of resveratrol doses was given to the monkeys, and the serum was analyzed via HPLC. The 40 mg dose of resveratrol gave equivalent levels of 3-*O*-glucuronide as determined in mice. The resveratrol was used to formulate a flavored primate treat (Bi-Serv, Frenchtown, NJ) and given to the monkeys prior to each meal. Thus, the monkeys received a total dose of 80 mg per day. All monkeys, regardless of weight, received the same amount of resveratrol. Monkeys in non-resveratrol groups receive a placebo treat.

Following one year on a relatively low dose, resveratrol was increased to 240 mg twice daily, or 480 mg per day, to document a dose-response effect. All measurements of interest and biopsy samples were collected at the two doses. Although the second dose was 6 times higher than the original 80 mg per day, no adverse effects were observed for the duration of the study. Measurement of trans-resveratrol and its *O*-sulfated metabolite in serum has been recently reported ((Jimenez-Gomez et al., 2013).

Physiological Measures

Body weight and waist measurement was determined in anesthetized monkeys (Ketamine, 7-10 mg/kg, IM or Telazol, 3-5 mg/kg, IM). Abdominal circumference was measured at the level of the umbilicus while the monkey was held in a prone position. Blood samples were obtained by venipuncture of the femoral vein using a vacutainer and vacuum tubes. Serum was collected and stored at -80 ^{o}C until assayed. Serum samples were analyzed with the VAP Cholesterol Test, a direct measure of comprehensive lipid assessment (Atherotech Diagnostics Lab, Birmingham, AL).

Pulse Wave Velocity

Cardiovascular exams were conducted in anesthetized monkeys following standard sedation (Telazol, 3-5 mg/kg, IM following an overnight fast, 16 hours). Telazol is a commonly used veterinary anesthetic producing a stable anesthesia plane with minimal cardiovascular effects. Heart rate, systolic and diastolic arterial blood pressures were recorded noninvasively with an automated sphygmomanometer cuff on the upper left arm (Dinamap, Critikon, Tampa, FL). PWV was derived from simultaneous recordings of

arterial flow waves from the left common carotid artery and the left femoral artery by using nondirectional transcutaneous Doppler flow probes (model 810A, 10 and 9 MHz, Parks Medical Electronics, Aloha, OR). A minimum of three serial readings were recorded and processed by an investigator blinded to the animal identification. An average value was calculated for each time point.

Euthanasia and Tissue Collection

Anesthesia was induced with Ketamine (7-10 mg/kg, IM) and, following blood collection, the monkeys were deeply anesthetized with a lethal dose of sodium pentobarbital (50 mg/kg, IP). Once maximally sedated, the monkeys were perfused with cold lactated Ringer's solution until death. Tissues were harvested immediately.

Histochemistry, Immunohistology and Morphometric Analysis

For 4 consecutive 5-7 μm paraffin embedded aortic cross-sections, we performed Elastica van Gieson (EVG) (to determine elastin fibers), CD68 (to determine cellular inflammation), CD31 (to determine endothelial cells), and Masson Trichrome staining (to determine extracellular matrix). For 4-6 consecutive 10 μm frozen aortic cross-sections, we performed Oil O Red (to determine fat deposits) and Alizarin Red staining (to determine calcium deposits), according to the modified protocols as reported in prior studies (Jiang et al., 2012; Wang et al., 2007; Wang et al., 2012).

High-resolution digital images of a representative cross-sectional section of stained thoracic aorta were acquired through a Leica microscope. Morphometric evaluation was performed using computerized imaging analysis system (Metamorph, University Imaging) by two investigators who were blinded to the treatment protocol. The intima area of the thoracic area (IA), corresponding to the layer between the lumen of surface and internal elastic laminae (IEL), was measured from an image taken at X200 magnification. Thoracic medial area (MA) was calculated from the IEL to external elastic laminae (EEL) from an image taken at X50 magnification.

Quantification of thoracic fat deposits (FA) and calcification area (CA, calcium deposits) were taken from images at X50 as well as inflammatory area (CD68A stained) from images taken at X100 and were expressed as the proportion of stained area to target area (density). The number of CD31-positive cells attached to a basement lamina was normalized by measurement of the circumference and were counted from 3-4 consecutive 5 μm paraffin cross-sections (X400).

Semi-quantification of histochemical staining was based on the extent of intimal involvement with a lipid deposition (Oil Red O staining) (Frink, 2002) (Suppl. Table 3):

Score 0: no or light (scattered) or clustered or diffused lipid deposits < 25%;

Score 1: clustered or diffused lipid deposits ≥25%, but <50%;
Score 2: clustered or diffused lipid deposits ≥50, but<75%;
Score 3: clustered or diffused lipid deposits≥75% or plaque alone.

Grading of calcium deposits according to the extent of arterial wall involvement with a calcium deposition (Alizarin Red staining) (Suppl. Table 3):
Score 0: no or light (scattered) or clustered or diffused calcium deposits < 25%;
Score 1: clustered or diffused calcium deposits ≥25%, but <50%;
Score 2: clustered or diffused calcium deposits ≥50, but<75%;
Score 3: clustered or diffused calcium deposits≥75%.

Immunohistochemical staining of local inflammatory molecules ICAM-1, VCAM-1 and MCP-1 was performed by modification of the semiquantitative method previously described (Raghunath et al., 1995; Wang and Lakatta, 2002) utilizing light microscopy at 100 X. In brief, primary antibodies against human ICAM-1 (rabbit, Santa Cruz Biotechnology, Santa Cruz, CA), VCAM-1 (rabbit, Santa Cruz), and MCP-1 (mouse, Santa Cruz) were employed each at 1:100 dilution, and a score/grade of 0 to 3 was used to indicate the relative total staining of cells plus matrix within the intimal or medial compartment, respectively.
Score 0: no staining (background) to <25% stained in that particular compartment;
Score 1: ≥25% to <50%;
Score 2: ≥50% to 75%;
Score 3: ≥75% to 100%.

cDNA Microarray Analysis

RNA was isolated from rhesus monkey aorta at 24-months of dietary intervention using Trizol reagent (Invitrogen) and further purified using RNeasy mini columns (Qiagen). For microarray analysis, RNA was processed, labeled and hybridized to (Illumina HumanHT-12 V4.0 expression beadchip using standard Illumina protocols) (by following protocols listed on the Gene Expression and Genomics Unit website at the National Institute on Aging, http://www.grc.nia.nih.gov/branches/rrb/dna/index/protocols.htm. Raw data were subjected to Z normalization to ensure compatibility using the formula: z(raw data)=[ln (raw data) – avg(ln(raw data))]/[std dev(ln (raw data))], where ln is natural logarithm, avg is the average over all genes of an array, std dev is the standard deviation over all genes of an array (Cheadle et al., 2003). The Z ratio (between treatment A and B) is given by z(A)-z(B)/std dev. Individual genes with Z ratio > 1.5 in both

directions, *P* value < 0.05, and false discovery rate > 0.3 were considered significantly changed. The number of samples for each group was: SD (4), HFS (9), and HFS+R (9). RNA preps for one HFS and one HFS+R monkey were not usable.

For parametric analysis of gene set enrichment (PAGE), a list of pathways was obtained from http://www.broad.mit.edu/gsea/msigdb/msigdb_index.html (C2 collection). Our expression data were tested for gene set enrichment using the PAGE method as previously described (Kim and Volsky, 2005). In brief, for each pathway, a Z score was computed as Z (pathway) = (sm mu)*pow(m,0.5)/delta, where mu = mean Z score of all gene symbols on the microarray, delta = standard deviation of Z scores of all gene symbols on the microarray, sm = mean Z score of gene symbols comprising one pathway present on the microarray, and m = no of gene symbols in a pathway present on the microarray. For each Z (pathway), a *P* value was also computed in JMP 6.0 to test for the significance of the Z score obtained. These tools are part of DIANE 6.0 and are available at http://www.grc.nia.nih.gov/branches/rrb/dna/diane_software.pdf. Gene expression data was deposited in Gene Expression Omnibus (Accession Number GSE45927).

Total RNA Isolation and Real Time Quantitative RT-PCR Assay

Samples of frozen aortic tissue from rhesus monkeys were mechanically disrupted in TRIzol® reagent (Applied Biosystems/Ambion, Austin, TX). Total RNA was extracted using the RiboPure™ kit (Applied Biosystems/Ambion) following the manufacturer's instructions. Subsequently, total RNA was converted to cDNA with the High Capacity cDNA reverse transcription kit (Applied Biosystems, Foster City, CA), and quantitative RT-PCR was carried out with SYBR® Green PCR master mix to quantitate the expression levels of GAS6, DHCR24, MYH11, and CRP2 on an ABI Prism 7300 sequence detection system (Applied Biosystems). GAPDH was selected as a housekeeping gene, as its expression was not significantly different between samples. Real-time PCR data were analysed by the ΔΔCT method. The expression of target genes was normalized to that of the housekeeping gene. All measurements were performed in duplicate. Controls consisting of reaction mixture without cDNA were negative in all runs. Fidelity of the PCR was determined by melting temperature analysis.

Human CAECs treated with 10% monkey serum were lysed and RNA was collected for quantitative RT-PCR assay. Analysis of mRNA expression of Nrf2 (*NFE2Ll2*) and the Nrf2/ARE target genes, heme oxygenase-1 (*HMOX1*) and γ-glutamylcysteine synthetase (*GCLC*), was carried out using a Stratagene MX3000 thermocycler, as previously reported (Ungvari et al., 2010; Ungvari et al., 2011). Amplification efficiencies were determined using a dilution series of a standard human CAECs sample. Quantification was performed using the ΔΔCT method. The relative quantities of the reference gene *Hprt* were used for internal normalization. Oligonucleotides used for quantitative RT-PCR are listed in Table S11.

Monocyte Adhesion Assay

Adhesion of fluorescently-labeled human monocytic (THP-1) cells to confluent monolayers of human CAECs was measured using a microplate-based assay, as reported (Csiszar et al., 2006). In brief, serum-treated human CAECs were grown to confluence in 96-well plates. THP-1 cells were labeled with the fluorescent dye BCECF (5 μmol/L final concentration; Molecular Probes, Eugene. OR) in serum-free RPMI medium for 45 min at 37 °C, were washed twice with prewarmed RPMI, and then treated with 1 μM of phorbol myristate acetate (PMA, Sigma-Aldrich, St-Louis, MO). PMA-treated, fluorescently labeled THP-1 cells (5 x 10^5 cells/well) were added to the 96-well plates containing confluent human CAECs. After a 45-min at 37 ^oC, nonadherent THP-1 cells were removed by careful washing with prewarmed RPMI and then 200 μL of PBS was added to each well. Fluorescence was measured using a fluorescent plate reader (excitation: 485 nm; emission: 528 nm). Controls included measurement of total fluorescence of labeled THP-1 cells before adhesion, controls for measuring autofluorescence of unlabeled cells, and measurement of monocyte adhesion to endothelial cell-free microplate wells. Samples were run in quadruplicates. Data are presented as background-corrected fluorescence units.

SILAC Labeling and Mass Spectrometry

Primary descending aortic vascular smooth muscle (VSM) cells were maintained in DMEM media (Invitrogen) supplemented with 10% dialyzed fetal bovine serum and 1% penicillin-streptomycin (Invitrogen). Customized arginine- and lysine-free DMEM media was obtained from AthenaES (Baltimore, MD). L-lysine-D_4 (K4), L-lysine-U-$^{13}C_6$,$^{15}N_2$ (K8), L-arginine-U-$^{13}C_6$ (R6) and L-arginine-U-$^{13}C_6$,$^{15}N_4$ (R10) were purchased from Cambridge Isotope Laboratories (Andover, MA). For isotopic SILAC labeling studies, VSM cultures were grown for 7 days (five division cycles) in DMEM media containing medium (M: K4,R6) or heavy (H: K8,R10) forms of arginine and lysine. Approximately 92% amino acid labeling was achieved using this protocol. To avoid non-labeled peptide errors, experiments were performed as triplets (SD vs. HFS or HFS+R diet) with random SILAC labeling comparing M and H conditions to the non-labeled 'light' (L) condition. Cellular protein extraction was performed with a standardized lysis buffer: 8M urea, 50 mM Tris.HCl, pH 8.0, 75 mM NaCl, 1 mM NaF, 1 mM β-glycerophosphate, 1 mM sodium orthovanadate, 10 mM sodium pyrophosphate, 1 mM phenylmethanesulfonylfluoride and a protease inhibitor cocktail (Roche Diagnostics). Protein lysate concentrations were determined by BCA protein assay kit (Thermo Fisher Scientific), and equal amounts of protein from M or H conditions were mixed to prepare the SILAC doublet mix. Proteins were reduced in 10 mM dithiothreitol at room temperature (RT) for 30 min and alkylated with 25 mM iodoacetamide at RT for 20 min in the dark. The reaction was quenched with an additional incubation in 15 mM

dithiothreitol at RT for 15 min. Protein extracts were diluted in 50 mM Tris.HCl, pH 8.0, to a final concentration of 1.5 M urea and were digested at 37 ºC using sequencing grade trypsin (Promega) at a 1:100 ratio (trypsin/protein, w/w). After overnight digestion, formic acid was added to a final concentration of 0.5% (v/v) and the peptide samples were desalted using Sep-Pak Vac C18 cartridges. Cartridges were washed with acetonitrile (ACN) and equilibrated with 0.1% formic acid. After loading peptides, cartridges were washed again with 0.1% formic acid. Peptides were then eluted with 70% ACN/0.1% formic acid, dried but not completely in SpeedVac (Thermo Fisher Scientific), and stored at -80 ºC.

To resolve peptides for subsequent quantitative analysis, strong cation exchange separation was performed prior to MS injection. LC-MS/MS analysis of trypsin-digested peptides was carried out using the LTQ/Orbitrap XL linear ion trap (Thermo Fisher Scientific). Peptides (1-2 µg) were first loaded onto a trap cartridge (Zorbax 300SB-C18, 5 µm, 0.3x5mm, Agilent) at a flow rate of 2 µl/min. Trapped peptides were then eluted onto a reversed-phase PicoFrit column (Betabasic 5µm C18, 150Å, 10 cm bed length, 360 od/75 id, New Objective) using a linear gradient of CAN (2-35%) containing 0.1% formic acid. Gradient duration was 80 min at a flow rate of 0.25 µl/min, followed by 80% ACN washing for 5 min. Eluted peptides were introduced, via nanospray, to the LTQ-Orbitrap. Spray voltage and ion transfer tube temperature were set at 1.8 kV and 180 ºC, respectively. Data-dependent acquisition mode was enabled, and each survey MS scan was followed by four MS/MS scans with dynamic exclusion option on. Full-scan MS survey spectra (m/z 300-2,000) in profile mode were acquired in the Orbitrap (resolution: 60,000; AGC target: 5E+05; max. fill time: 500 ms). The four most intense peptide ions from the survey scan were fragmented by collision-induced dissociation (normalized collision energy: 35%; activation Q: 0.250; activation time: 30 ms) in the LTQ (AGC target: 1E+04; max. fill time: 200 ms). Precursor ion-charge state screening was used to reject unassigned charge states. The dynamic exclusion list was restricted to a maximum of 500 entries with maximum exclusion duration of 90 s and a relative mass tolerance window of ±10 ppm. Raw data were analyzed using MaxQuant (version 1.1.1.6). Retention time-dependent mass calibration was applied and peak lists were searched against a database containing all 87,061 entries from the International Protein Index human protein database (http://www.ebi.ac.uk/IPI/IPIhelp.html) version 3.68 and 262 frequently observed contaminants as well as the reversed sequences of all entries. Database searches were performed with the following settings: (1) precursor and fragment ion peaks were searched with mass tolerance of 7 ppm and 0.5 kDa, respectively; (2) enzyme specificity was set to trypsin/IP; (3) up to two missed cleavages were allowed and only peptides with at least 6 amino acids in length were considered; and (4) carbamidomethylcysteine and oxidation on methionine were set as fixed and variable modifications, respectively. Using a decoy database strategy, peptide identifications were accepted based on their posterior error probability (PEP),

until less than 1% reverse hits were retained in the list. SILAC ratios from MaxQuant were converted to $\log_2$-scale and the mean and standard deviation of the dataset were calculated with SigmaPlot v11.0. The correlation curve of measured vs. pre-defined mixed ratios and its coefficients were obtained by linear regression (SigmaPlot), and the dataset's standard deviations were used for error bar calculations for each data point.

Protein Expression Analysis

SILAC proteomic results were validated by Western blots using standard methodologies. In brief, rhesus monkey aortic tissues were homogeneized using sonication followed by subcellular fractionation using a Qiagen Q-proteome kit according to the manufacturer's instructions (Qiagen, Inc., Valencia, CA). For all experiments, cytoplasmic fractions were used. Each protein extract was loaded onto a BisTris 4-12% polyacrylamide gel (Invitrogen) before electrotransfer to a PVDF membrane (Thermo Scientific, Rockford, IL). Proteins were identified using primary antibodies at 1:1000 dilutions, followed by species-specific alkaline phosphatase-conjugated secondary antibodies (Sigma-Aldrich) at a 1:7000 dilution. Primary antibodies specific for SERPINE 1 (serpin peptidase inhibitor, clade E member 1) and CTNNB1 (cadherin-associated protein β-1, 88kDa) were obtained from Sigma Aldrich (St. Louis, MO). Primary antibodies specific for GAP-43 (anti-growth associated protein-43) and ROCK2 (Rho-associated protein kinase 2) were obtained from Abcam (Cambridge, MA). Primary antibodies specific for CAV1 (caveolin-1) and MAP2 (microtubule-associated protein 2) were purchased from Cell Signaling Technology (Danvers, MA), whereas anti-synaptopodin (SYNPO) antibody was obtained from Santa Cruz. PVDF-bound immune complexes were identified using enzyme-linked chemifluorescence and quantified using a Typhoon 9410 PhosphorImager (GE Healthcare). All antibodies used have been previously validated.

Bioinformatic Analysis

SILAC-derived protein lists were analyzed using multiples forms of functional annotational clustering, i.e. Gene Ontology (GO - http://www.geneontology.org/), Parametric Analysis of Geneset Enrichment (KEGG - http://www.genome.jp/kegg/; WikiPathways - http://www.wikipathways.org/index.php/WikiPathways; PathwayCommons - http://www.pathwaycommons.org/pc/), and Latent Semantic Indexing (LSI). A cutoff of at least two proteins from the original filtered/analyzed datasets was set in order to fully populate a GO term or a KEGG/WikiPathways/PathwayCommons signaling pathway, with a probability (p) of enrichment value of ≤ 0.05. These Parametric Geneset enrichment analyses are primarily performed using raw datasets to test significance of enrichment at a group/collection level rather than at the individual gene/protein significance level (Mootha et al., 2003). From our SILAC analysis we found 121 proteins that were

reliably identified (n>2 peptides sequenced per identified protein) in all of experimental datasets (SD, HFS, HFS+R) and demonstrated a significant alteration in at least one of the experimental (HFS, HFS+R) datasets as compared to SD control. This list was used for bioinformatic interrogation employing GO Biological Process (GO-bp), KEGG, WikiPathways and PathwayCommons enrichment analysis. For each significantly enriched GO term group or signaling pathway, a combinatorial '*hybrid*' score was calculated as follows: GO/pathway enrichment factor * negative $\log_{10}$(enrichment probability). The percentage distribution of the hybrid scores for all the significantly regulated GO term groups or signaling pathways was then represented in a pie chart (Suppl. Figure S2B). Moreover, to reveal the most important functional proteins that regulate the diverse forms of signaling within the SILAC list, LSI analysis (GeneIndexer: Computable Genomix, Memphis, TN) was employed as described previously (Chadwick et al., 2012). LSI interrogator terms related to cardiovascular and cellular structural signaling (derived from the GO/signaling pathway enrichment analysis) were used to interrogate a complete human genomic dataset (LSI terms: atherosclerosis; calcium; contractility; cytoskeleton; elasticity; focal adhesion; integrin; polymerization; proliferation; sarcoplasmic reticulum; tyrosine kinase). Nineteen proteins from the sixty-four filtered SILAC list demonstrated an implicit correlation to all of the previously mentioned input LSI interrogator terms (Suppl. Fig. S2C).

Tissue Transglutaminase (TGM2) Activity Assay

TGM activity was determined using the 5-(biotinamido)pentylamine (BPA) incorporation assay as described in detail elsewhere (Jandu et al., 2013; Santhanam et al., 2010). In brief, cells were grown to confluence and media was exchanged for phenol red free DMEM supplemented with 2% serum. Media was then supplemented with a final concentration of 100 µM BPA (ThermoFisher) and 1 mM $CaCl_2$, and cells were incubated in a humidified incubator (37^{o}C, 5% CO_2). After 3 h, cells were washed 3x with PBS, followed by cell lysis using RIPA buffer (Upstate) containing protease inhibitors (Roche), centrifugation at 12,000 rpm for 5 min, and detection of protein concentration in the supernatants (BioRad Protein Assay Reagent). Proteins (0.5 µg) from each sample were then loaded onto nitrocellulose membrane using a BioRad Dot Blot setup. The membrane was blocked overnight in 3% BSA in TBST, rinsed 3x with TBST, and incubated with streptavidin-HRP conjugate (GE Healthcare; 1:10,000; 1% BSA; 2 h). The dot blot was rinsed 3x in TBST, developed (West Pico Chemiluminescence substrate; Pierce), and quantified using ImageJ software (NIH).

Statistical Analyses

PWV, body weight, and serum cholesterol repeated measures data were analyzed using linear mixed-effects models. A group or group*time interaction were considered statistically significant at $p \leq 0.05$.

For histochemistry measures, a one-way ANOVA was done to compare mean values for the SD, HFS and HFS+R groups. Pairwise comparisons were made using the Bonferroni's Multiple Comparison Test. Data are presented as mean $\pm$ SEM.

In each Western blot histogram, data represent the means ± S.E. Statistical analyses (Student's *t* test) were performed using GraphPad Prism (GraphPad Software, San Diego, CA). *p*-values less than 0.05 were considered statistically significant.

Table S1, related to Figure 1. Baseline characteristics of rhesus monkeys.

Diet Group	N	Age (yr)	Weight (kg)	Waist (cm)	Glucose (mg/dL)	TGs (mg/dL)	PWV (cm/sec)
SD	4	9.8 ± 0.8	12.98 ± 1.2	42.0 ± 4.2	58.77 ± 1.14	73.0 ± 27.4	1677 ± 413
HFS	10	11.0 ± 0.6	13.24 ± 1.1	40.8 ± 3.3	60.07 ± 2.75	65.4 ± 15.4	1321 ± 135
HFS+R	10	10.3 ± 0.5	12.82 ± 0.8	41.1 ± 3.4	61.24 ± 1.04	70.1 ± 12.6	1360 ± 152

TG: Triglycerides; PWV: Pulse Wave Velocity. Values represent mean ± SEM.

Table S2, related to Figure 2. Weight and dimensions of the heart and aortic remodeling following 2 years on study

	SD (n=4)	HFS (n=10)	HFS+R (n=10)
Body weight (BW) (kg)	13.49 ± 1.31	16.69 ± 1.8	15.70 ± 1.12
Heart weight (HW) (gr)	50.01 ± 1.2	59.55 ± 4.9	54.38 ± 1.9
HW/BW (g/kg)	3.82 ± 0.4	3.76 ± 0.3	3.57 ± 0.2
L (cm)	5.67 ± 0.33	5.70 ± 0.3	5.21 ± 0.2
LVFT (cm)	1.47 ± 0.3	1.07 ± 0.2	0.96 ± 0.2
LVPT (cm)	1.00 ± 0.0	0.80 ± 0.2	0.69 ± 0.2
LVAT (cm)	0.87 ± 0.03	0.80 ± 0.2	0.66 ± 0.1
IVST (cm)	0.93 ± 0.1	0.80 ± 0.1	0.75 ± 0.1
RVT (cm)	0.33 ± 0.03	0.33 ± 0.04	0.30 ± 0.03
Aortic Remodeling Measurements			
IA (μm^2)	6788 ± 3655	6132 ± 3867	5508 ± 2530
MA (μm^2)	161692 ± 20667	171900 ± 50628	150224 ± 31743
LA (μm^2)	207722 ± 51418	384949 ± 511158	207850 ± 59814
ECM (μm^2)	31779 ± 18002	40793 ± 14569	40203 ± 22641
Semi-quantification scoring for fat deposition and calcification of the thoracic aorta			
Fat deposition	0.5 ± 0.29	2.2 ± 0.29*	1.1 ± 0.31
Calcification	2.0 ± 0.58	2.7 ± 0.15**	1.7 ± 0.15

L=long axis of left ventricle (LV); LVFT: LV free wall thickness; LVPT: LV posterior thickness LVAT: LV anterior wall thickness; IVST=intra-ventricular septum thickness: RVT: right ventricular anterior thickness; IA: intimal area; MA: medial area; LA: lumen area; ECM: extracellular matrix area (5X0). Values represent Mean ± SEM.

*P<0.008 HFS compared to SD and HFS+R

**P<0.007 HFS compared to HFS+R

Table S3A , related to Figure 3B - List of shared GO terms that were significantly affected both by HFS vs. SD and resveratrol in HFS+R vs. HF. This table provides a list of the Z-scores values of both comparisons HFS vs. SD and resveratrol in HFS+R vs. HF

Table S3B, related to Figure 3C- List of genes whose expression in HFS diet was reversed upon resveratrol supplementation. This table provides a complete list of all the genes that were reversed by resveratrol. Criteria for significance were as followed: z ratio > 1.5 in both directions; P value < 0.05; fdr < 0.3.

Table S3C, related to Figure 4A - SILAC-based identification and quantitation of relative differential changes in protein expression from a primary culture of rhesus monkey vascular smooth muscle cells. Fold change expression data are represented for proteins identified in a 7-day primary culture of VSM cells prepared from rhesus monkey fed either HFS diet or HFS supplemented with resveratrol (HFS+R), as compared to standard diet-fed animals (SD). Fold change values in red indicate an upregulation (non-bold, P<0.05; bold, P<0.01), while fold changes in green denote a downregulation (non-bold, P<0.05; bold, P<0.01). Fold change values in black represent expression changes that were not statistically significant. Bullets refer to proteins –and gene symbols- highlighted in Fig. 4, panel A.

Table S4, related to Figure 4A - Enrichment analysis of proteins that are significantly regulated by HFS/HFS+R within GO term-Biological Process, KEGG signaling pathways, WikiPathways, and PathwayCommons. The table provides the number of reference proteins in the category (C) related to the designated term/pathway, number of proteins from the input dataset in this specific category (O), the expected number in the specific category (based on a whole-genomic expression frequency) scaled appropriately for the size of the input dataset compared to the whole background genome seat (E). Simple division of O/E results in the relative enrichment ratio (R) of the term/pathway group by the proteins from the input dataset. The p value for this enrichment is generated initially with a hypergeometric test, which is then modified by multiple test adjustment (P). A hybrid (H) term/pathway score is created by multiplication of R with the negative $\log_{10}$ of P.

GO term – biological process	C	O	E	R	P	H
Collagen fibril organization	26	5	0.16	30.37	5.39E-05	129.6316
Cellular aldehyde metabolic process	28	5	0.18	28.2	5.60E-05	119.9011
Collagen biosynthetic process	15	3	0.09	31.58	0.0017	87.46242
Antigen processing and presentation of peptide antigen via MHC class I	17	3	0.11	27.87	0.0027	71.58789
Regulation of microtubule cytoskeleton organization	32	4	0.2	19.74	0.0012	57.65696
Extracellular matrix organization	93	7	0.59	11.89	0.0001	47.56
Extracellular structure organization	159	8	1.01	7.95	0.0003	28.00689
Cytoskeleton organization	469	15	2.97	5.05	4.26E-05	22.07148
Response to oxidative stress	159	7	1.01	6.95	0.0015	19.62617
Muscle organ development	265	9	1.68	5.36	0.0012	15.65559
Blood vessel development	274	9	1.74	5.19	0.0014	14.8116

Wound healing	194	7	1.23	5.7	0.0027	14.64123
Anatomical structure morphogenesis	1223	24	7.74	3.1	5.33E-05	13.24715
Cellular component organization	2566	39	16.25	2.4	6.76E-06	12.40813
Cell adhesion	785	17	4.97	3.42	0.0003	12.04825
Response to stress	1696	24	10.74	2.23	0.0017	6.176099

KEGG Pathway	**C**	**O**	**E**	**R**	**P**	**H**
ECM-receptor interaction	84	11	0.21	52.54	6.13E-15	746.7268
Focal adhesion	201	15	0.5	29.94	2.01E-16	469.9623
Histidine metabolism	29	4	0.07	55.34	6.43E-06	287.3136
Glycolysis / Gluconeogenesis	62	6	0.15	38.83	2.11E-07	259.2181
Sulfur metabolism	13	2	0.03	61.73	0.0013	178.1563
Fatty acid metabolism	42	4	0.1	38.21	2.33E-05	177.0133
Tyrosine metabolism	46	4	0.11	34.89	3.03E-05	157.6525
Metabolism of xenobiotics by cytochrome P450	70	5	0.17	28.66	6.43E-06	148.7967
Butanoate metabolism	34	3	0.08	35.4	0.0003	124.7099
Phenylalanine metabolism	22	2	0.05	36.48	0.0031	91.51513

Drug metabolism - cytochrome P450	72	4	0.18	22.29	0.0001	89.16
Type I diabetes mellitus	44	3	0.11	27.36	0.0006	88.14978
Ascorbate and aldarate metabolism	25	2	0.06	32.1	0.0037	78.06072
Vascular smooth muscle contraction	115	5	0.29	17.44	5.45E-05	74.35725
Regulation of actin cytoskeleton	216	6	0.54	11.15	8.25E-05	45.53154
WikiPathways	**C**	**O**	**E**	**R**	**P**	**H**
Fatty acid omega oxidation	14	3	0.03	85.98	3.23E-05	386.1188
Sulfation	17	3	0.04	70.81	4.80E-05	305.8113
Inflammatory response pathway	30	4	0.07	53.5	1.14E-05	264.4556
Focal adhesion	185	11	0.46	23.86	3.77E-11	248.7085
G13 signaling pathway	40	3	0.1	30.09	0.0004	102.244
Estrogen metabolism	23	2	0.06	34.89	0.004	83.66413
Regulation of actin cytoskeleton	143	6	0.36	16.83	1.36E-05	81.90254
Prostaglandin synthesis and regulation	31	2	0.08	25.89	0.0059	57.71264
Senescence and autophagy	60	3	0.15	20.06	0.0017	55.55719
Proteasome degradation	64	3	0.16	18.81	0.0018	51.62832
Retinol metabolism (BiGCaT, NuGO)	37	2	0.09	21.69	0.0078	45.72047
TGF beta signaling pathway	100	3	0.25	12.04	0.0048	30.46953
Integrin-mediated cell adhesion	133	3	0.33	9.05	0.0085	27.91786
Adipogenesis	52	2	0.13	15.43	0.0106	18.73876
Delta-notch signaling pathway	86	2	0.21	9.33	0.0235	15.19794
PathwayCommons signaling pathway	**C**	**O**	**E**	**R**	**P**	**H**
Collagen-mediated activation cascade	7	2	0.02	114.64	0.0006	369.3527
VEGFR3 signaling in lymphatic endothelium	23	4	0.06	69.78	2.34E-05	323.1361
Ethanol catabolism	8	2	0.02	100.31	0.0009	305.5199
Platelet activation triggers	18	3	0.04	66.87	0.0002	247.3501
Platelet adhesion to exposed collagen	10	2	0.02	80.25	0.0013	231.606
Platelet activation	74	5	0.18	27.11	4.65E-05	117.4554
Cell surface interactions at the vascular wall	66	4	0.16	24.32	0.0002	89.95895
Integrin cell surface interactions	67	4	0.17	23.95	0.0002	88.59033
Regulation of insulin secretion by acetylcholine	26	2	0.06	30.86	0.0059	68.79151
ATM mediated response to DNA double-strand break	26	2	0.06	30.86	0.0059	68.79151
Hemostasis	171	6	0.43	14.08	8.94E-05	57.00517
Integrins in angiogenesis	63	3	0.16	19.11	0.0021	51.17239
Biological oxidations	118	4	0.29	13.6	0.0009	41.4223
IFN-gamma pathway	342	5	0.85	5.87	0.0059	13.0851
Regulation of cytoplasmic and nuclear SMAD2/3 signaling	265	4	0.66	6.06	0.0116	11.72938

Table S5, related to Figure 3D. List of oligonucleotide primer sets for real-time quantitative RT-PCR

mRNA targets	GeneBank number	Primer sequence
Gas6	XM_002800847.1 M. mulatta	Left: 5'-CCAAGAAACGGTGAAAGCGAACA-3' Right: 5'-CGGATGTGAGCCACGACTTCTATT-3'
Dhcr24	XM_001108186.2 M. mulatta	Left: 5'-GCCGCTGTCGCTCATCTTCG-3' Right: 5'-GTCTTGCTGCCCTGCTCCTT-3'
Crp2	XM_001082599.2 M. mulatta	Left: 5'-GGTGAAATCTATTGTAAAGGATGC-3' Right: 5'-TACTGGGCATGAACAAGAGC-3'
Myh11	XM_001109463.2 M. mulatta	Left: 5'-CGCCAAGAGACTCGTCTGG-3' Right: 5'-TCTTTCCCAACCGTGACCTTC-3'
Gapdh	NM_001195426.1 M. mulatta	Left: 5'-TGAAGCAGGCGTCGGAGGG-3' Right: 5'-CGAAGGTGGAAGAGTGGGTG-3'
NFE2L2	NM_006164 H. sapiens	Left: 5'-CAACTCAGCACCTTATATCTC-3' Right: 5'-TTCTTAACATCTGGCTTCTTAC-3'
GCLC	NM_001498 H. sapiens	Left: 5'-CAGTGGTGGATGGTTGTG-3' Right: 5'-ATTGATGATGGTGTCTATGC-3'
HMOX1	NM_002133 H. sapiens	Left: 5'-AAGTATCCTTGTTGACACG-3' Right: 5'-TGAGCCAGGAACAGAGTG-3'
HPRT	NM_000194 H. sapiens	Left: 5'-CCGTGTGTTAGAAAAGTAAGAAGC-3' Right: 5'-AACTGCTGACAAAGATTCACTGG-3'

Figure S1, related to Figure 3. Change in expression of select genes between HFS vs. SD and HFS+R vs. HFS. The data is depicted as Z-ratios.

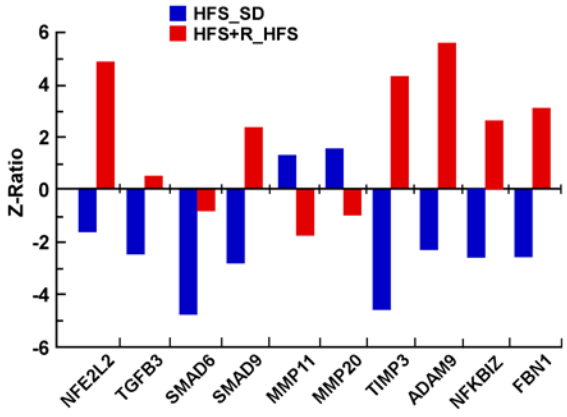

Figure S2, related to Figure 4. SILAC-based identification and quantitation of relative differential changes in protein expression from a primary culture of rhesus monkey vascular smooth muscle cells. (A) Multiple bioinformatic interpretation (GO-*bp*, KEGG, WikiPathways, PathwayCommons) of the 121 proteins reliably identified by SILAC labeling of a 7-day primary culture of rhesus monkey VSM cells across the SD, HFS and HFS+R cohorts. The relative percentage scores for the pie charts were created using the hybrid scores of pathway or GO term population depicted in Supplemental Tables 6-9. (B) Latent semantic indexing (LSI) heatmap analysis of multidimensional proteins associated with LSI interrogator terms associated with the bioinformatic-predicted functions of the 121-protein set. Implicit textual association between the specific protein from the input list (left of heatmap) and the user-defined LSI interrogator term (top of heatmap) is indicated by a red block while the lack of association is denoted by a black block. Nineteen 'multidimensional' proteins were associated with all of the interrogator terms.

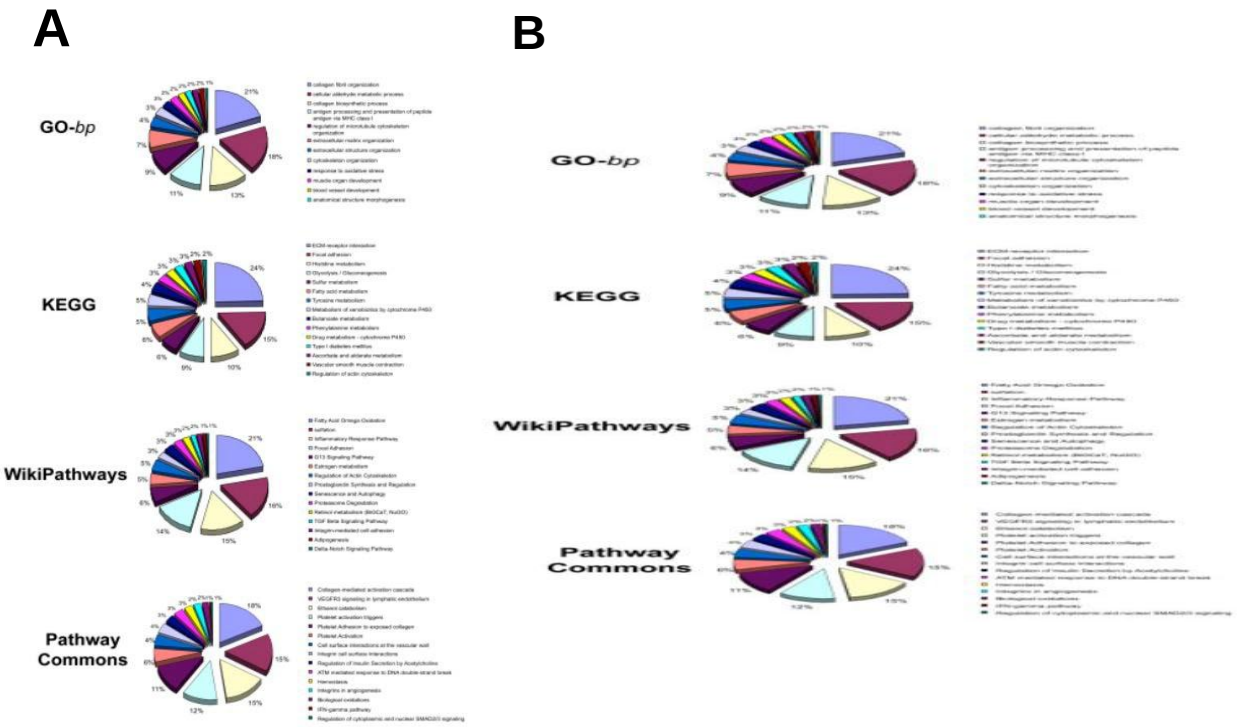

Figure S3, related to Figure 4. Tissue transglutaminase activity in primary culture of rhesus monkey vascular smooth muscle cells. TGM2 activity was measured using Dot blot assay and normalized to GAPDH.

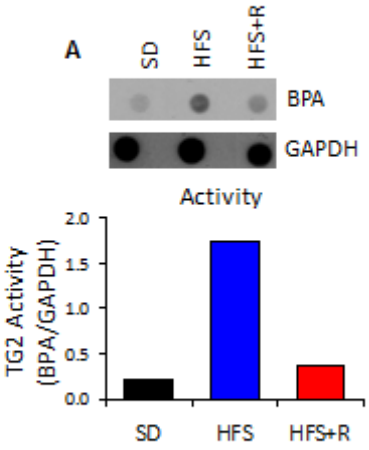

References

Baur, J.A., Pearson, K.J., Price, N.L., Jamieson, H.A., Lerin, C., Kalra, A., Prabhu, V.V., Allard, J.S., Lopez-Lluch, G., Lewis, K., Pistell, P.J., Poosala, S., Becker, K.G., Boss, O., Gwinn, D., Wang, M., Ramaswamy, S., Fishbein, K.W., Spencer, R.G., Lakatta, E.G., Le Couteur, D., Shaw, R.J., Navas, P., Puigserver, P., Ingram, D.K., de Cabo, R., and Sinclair, D.A. (2006). Resveratrol improves health and survival of mice on a high-calorie diet. Nature *444*, 337-342.

Chadwick, W., Martin, B., Chapter, M.C., Park, S.S., Wang, L., Daimon, C.M., Brenneman, R., and Maudsley, S. (2012). GIT2 acts as a potential keystone protein in functional hypothalamic networks associated with age-related phenotypic changes in rats. PLoS One *7*, e36975.

Cheadle, C., Vawter, M.P., Freed, W.J., and Becker, K.G. (2003). Analysis of microarray data using Z score transformation. J. Mol. Diagn. *5*, 73-81.

Csiszar, A., Ahmad, M., Smith, K.E., Labinskyy, N., Gao, Q., Kaley, G., Edwards, J.G., Wolin, M.S., and Ungvari, Z. (2006). Bone morphogenetic protein-2 induces proinflammatory endothelial phenotype. Am. J. Pathol. *168*, 629-638.

Deshpande, D.A., Wang, W.C., McIlmoyle, E.L., Robinett, K.S., Schillinger, R.M., An, S.S., Sham, J.S., and Liggett, S.B. (2010). Bitter taste receptors on airway smooth muscle bronchodilate by localized calcium signaling and reverse obstruction. Nat. Med. *16*, 1299-1304.

Frink, R.J. (2002). Inflammatory Atherosclerosis: Characteristics of the Injurious Agent. (Sacramento, CA: Heart Research Foundation).

Jandu, S.K., Webb, A.K., Pak, A., Sevinc, B., Nyhan, D., Belkin, A.M., Flavahan, N.A., Berkowitz, D.E., and Santhanam, L. (2013). Nitric oxide regulates tissue transglutaminase localization and function in the vasculature. Amino Acids *44*, 261-269.

Jiang, L., Zhang, J., Monticone, R.E., Telljohann, R., Wu, J., Wang, M., and Lakatta, E.G. (2012). Calpain-1 regulation of matrix metalloproteinase 2 activity in vascular smooth muscle cells facilitates age-associated aortic wall calcification and fibrosis. Hypertension *60*, 1192-1199.

Jimenez-Gomez, Y., Mattison, J.A., Pearson, K.J., Martin-Montalvo, A., Palacios, H.H., Sossong, A.M., Ward, T.M., Younts, C.M., Lewis, K., Allard, J.S., Longo, D.L., Belman, J.P., Malagon, M.M., Navas, P., Sanghvi, M., Moaddel, R., Tilmont, E.M., Herbert, R.L., Morrell, C.H., Egan, J.M., Baur, J.A., Ferrucci, L., Bogan, J.S., Bernier, M., and de Cabo, R. (2013). Resveratrol improves adipose insulin signaling and reduces the inflammatory response in adipose tissue of rhesus monkeys on high-fat, high-sugar diet. Cell Metab. *18*, 533-545.

Kim, S.Y., and Volsky, D.J. (2005). PAGE: parametric analysis of gene set enrichment. BMC Bioinformatics 6, 144.

Mootha, V.K., Lindgren, C.M., Eriksson, K.F., Subramanian, A., Sihag, S., Lehar, J., Puigserver, P., Carlsson, E., Ridderstrale, M., Laurila, E., Houstis, N., Daly, M.J., Patterson, N., Mesirov, J.P., Golub, T.R., Tamayo, P., Spiegelman, B., Lander, E.S., Hirschhorn, J.N., Altshuler, D., and Groop, L.C. (2003). PGC-1alpha-responsive genes involved in oxidative phosphorylation are coordinately downregulated in human diabetes. Nat Genet 34, 267-273.

Raghunath, P.N., Tomaszewski, J.E., Brady, S.T., Caron, R.J., Okada, S.S., and Barnathan, E.S. (1995). Plasminogen activator system in human coronary atherosclerosis. Arterioscler Thromb Vasc Biol 15, 1432-1443.

Santhanam, L., Tuday, E.C., Webb, A.K., Dowzicky, P., Kim, J.H., Oh, Y.J., Sikka, G., Kuo, M., Halushka, M.K., Macgregor, A.M., Dunn, J., Gutbrod, S., Yin, D., Shoukas, A., Nyhan, D., Flavahan, N.A., Belkin, A.M., and Berkowitz, D.E. (2010). Decreased S-nitrosylation of tissue transglutaminase contributes to age-related increases in vascular stiffness. Circ Res 107, 117-125.

Wang, M., and Lakatta, E.G. (2002). Altered regulation of matrix metalloproteinase-2 in aortic remodeling during aging. Hypertension 39, 865-873.

Wang, M., Zhang, J., Jiang, L.Q., Spinetti, G., Pintus, G., Monticone, R., Kolodgie, F.D., Virmani, R., and Lakatta, E.G. (2007). Proinflammatory profile within the grossly normal aged human aortic wall. Hypertension 50, 219-227.

Wang, M., Zhang, J., Telljohann, R., Jiang, L., Wu, J., Monticone, R.E., Kapoor, K., Talan, M., and Lakatta, E.G. (2012). Chronic matrix metalloproteinase inhibition retards age-associated arterial proinflammation and increase in blood pressure. Hypertension 60, 459-466.